Conical Cavity for Surface Resistance Measurements of High Temperature Superconductors

Bernd Mayer, Andreas Reccius, and Reinhard Knöchel, *Senior Member, IEEE*

***Abstract*—A new conically-shaped cavity is presented which intrinsically avoids mode-degeneration while maintaining the advantages of cylindrical resonators. The cavity is applied to surface resistance measurements of YBaCuO thin films on MgO substrates at 18 GHz. The lowest measured value was 4.5 mΩ ± 2.1 mΩ for a 10 mm × 10 mm laser ablated film at 77 K. An error analysis is carried out which leads to an accuracy of ±2.1 mΩ for samples with 9 mm diameter and an accuracy of ±0.5 mΩ for samples with 20 mm diameter.**

I. Introduction

ONE OF the main characteristics of superconductors especially with regard to applications to components are the losses at microwave frequencies. A widely used measurement method to determine these losses is to replace a part of the surface of a microwave cavity by the sample and to measure the change in quality factor over temperature [1]–[4].

Commonly used are H_{0in}-mode cylindrical cavities because of their purely circumferential surface currents. Unfortunately, H_{0in}-modes are degenerated with E_{1in}-modes. These modes deteriorate the measurement accuracy considerably and have to be suppressed. To achieve this, rather tricky methods like circumferential grooves as "mode traps" or for instance the isolation of the endplates of the resonator are applied. The unwanted modes are either detuned or attenuated or both. However, all of these mode suppressors are introduced empirically by cut and try procedures, and seldom a complete suppression is obtained.

In order to arrive at a systematic approach in the design of a cavity for the above described purpose, a conically-shaped cavity, sketched in Fig. 1, is introduced. This cavity removes degeneracy intrinsically. The mode-spectrum of conical cavities for various inclination angles is calculated rigorously and several mode charts are given.

Another problem the paper deals with is due to imperfections of the feeding line connectors which lead to a systematic error in the measurements. This error can be reduced by using a newly developed deembedding process.

Manuscript received April 30, 1991; revised August 21, 1991. This work was supported by the Bundesministerium für Forschung und Technologie (BMFT-FKZ 13 N 57 06).

The authors are with Technische Universität Hamburg-Harburg, Arbeitsbereich Hochfrequenztechnik, Postfach 90 10 52, D-2100 Hamburg 90, Germany.

IEEE Log Number 9104776.

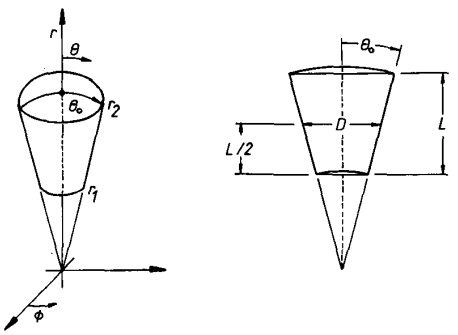

Fig. 1. Geometry of the cavity.

II. Theory

For the calculations a spherical coordinate system is used. The surface of the cavity is defined by the conditions:

$$r = r_1 \quad 0 < \theta < \theta_0 \quad 0 \leqq \Phi < 2\pi$$

$$r = r_2 \quad 0 < \theta < \theta_0 \quad 0 \leqq \Phi < 2\pi$$

$$\theta = \theta_0 \quad r_1 < r < r_2 \quad 0 \leqq \Phi < 2\pi.$$

The boundary value problem to be solved is fully defined by Maxwell's equations:

$$\vec{\nabla} \times \vec{E} = -j\omega\mu\vec{H}$$

$$\vec{\nabla} \times \vec{H} = j\omega\epsilon\vec{E} \tag{1}$$

and the boundary condition $E_t \equiv 0$ at the cavity surface.

It turns out, that the boundary conditions can be satisfied by using single wave functions Ψ^E or Ψ^H, defined by $\vec{A} = \vec{u}_r\Psi^E$ and $\vec{F} = \vec{u}_r\Psi^H$. I.e. purely transversal magnetic modes with respect to $\vec{u}_r$, which are denoted as E-modes and purely transversal electric modes, which are denoted as H-modes exist [5]. The wave functions are solutions of the differential equation:

$$\frac{\partial^2\Psi^{E,H}}{\partial r^2} + \frac{1}{r^2\sin\theta}\frac{\partial}{\partial\theta}\left(\sin\theta\frac{\partial\Psi^{E,H}}{\partial\theta}\right) + \frac{1}{r^2\sin^2\theta}\frac{\partial^2\Psi^{E,H}}{\partial\Phi^2} + k^2\Psi^{E,H} = 0, \tag{2}$$

where $k^2 = \omega^2\mu_0\epsilon_0$ denotes the wave number.

The field components can be deduced from

$$\vec{E} = -\vec{\nabla} \times \vec{F} + \frac{1}{j\omega\epsilon_0} \vec{\nabla} \times \vec{\nabla} \times \vec{A}$$

$$\vec{H} = \vec{\nabla} \times \vec{A} + \frac{1}{j\omega\mu_0} \vec{\nabla} \times \vec{\nabla} \times \vec{F}. \tag{3}$$

For the E-modes this yields in detail:

$$E_r = \frac{1}{j\omega\epsilon_0} \left(\frac{\partial^2}{\partial r^2} + k^2 \right) \Psi^E \quad H_r \equiv 0$$

$$E_\theta = \frac{1}{j\omega\epsilon_0 r} \frac{\partial^2 \Psi^E}{\partial r\, \partial\theta} \quad H_\theta = \frac{1}{r \sin\theta} \frac{\partial \Psi^E}{\partial \Phi}$$

$$E_\Phi = \frac{1}{j\omega\epsilon_0 r \sin\theta} \frac{\partial^2 \Psi^E}{\partial r\, \partial\Phi} \quad H_\Phi = \frac{-1}{r} \frac{\partial \Psi^E}{\partial\theta} \tag{4}$$

and for the H-modes:

$$E_r \equiv 0 \quad H_r = \frac{1}{j\omega\mu_0} \left(\frac{\partial^2}{\partial r^2} + k^2 \right) \Psi^H$$

$$E_\theta = \frac{-1}{r \sin\theta} \frac{\partial \Psi^H}{\partial \Phi} \quad H_\theta = \frac{1}{j\omega\mu_0 r} \frac{\partial^2 \Psi^H}{\partial r\, \partial\theta}$$

$$E_\Phi = \frac{1}{r} \frac{\partial \Psi^H}{\partial\theta} \quad H_\Phi = \frac{1}{j\omega\mu_0 r \sin\theta} \frac{\partial^2 \Psi^H}{\partial r\, \partial\Phi}. \tag{5}$$

Equation (2) can be solved by separation of variables. An appropriate general solution is given by

$$\Psi^{E,H} = \begin{Bmatrix} \sqrt{\frac{\pi kr}{2}}\, J_{\nu+1/2}(kr) \\ \sqrt{\frac{\pi kr}{2}}\, N_{\nu+1/2}(kr) \end{Bmatrix} \begin{Bmatrix} P_\nu^m(\cos\theta) \\ Q_\nu^m(\cos\theta) \end{Bmatrix} \begin{Bmatrix} \cos m\Phi \\ \sin m\Phi \end{Bmatrix} \tag{6}$$

where $J_{\nu+1/2}$, $N_{\nu+1/2}$ are solutions of Bessel's differential equation and P_ν^m, Q_ν^m are solutions of Legendre's differential equation [6].

Only integer m-values occur, because the full range of Φ from 0 to 2π is required. The $Q_\nu^m(\cos\theta)$ functions do not occur in the present field problem, because they are infinite at $\theta = 0$. The m values can be restricted to nonnegative values because the P_ν^m and P_ν^{-m} functions are linearly dependent and the ν values can be restricted to values greater than $-(1/2)$ because the P_ν^m and $P_{-\nu-1}^m$ functions are also linearly dependent, although some care must be taken in the case $P_\nu^{-m}(x)$ with $m > 0$, $\nu = n$ an integer and $n < m$ [6].

Hence the E-mode wave functions are

$$\Psi^E = H_0 \sqrt{\frac{\pi kr}{2}}\, (J_{\nu+1/2}(kr) + a \cdot N_{\nu+1/2}(kr)) \cdot P_\nu^m(\cos\theta) \cdot \begin{Bmatrix} \cos m\Phi \\ \sin m\Phi \end{Bmatrix} \tag{7}$$

and the H-mode wave functions are

$$\Psi^H = E_0 \sqrt{\frac{\pi kr}{2}}\, (J_{\nu+1/2}(kr) + b \cdot N_{\nu+1/2}(kr)) \cdot P_\nu^m(\cos\theta) \cdot \begin{Bmatrix} \cos m\Phi \\ \sin m\Phi \end{Bmatrix} \tag{8}$$

The unknowns a, b, k and ν can be calculated by using the boundary condition $E_t \equiv 0$ for the corresponding electrical field components. Considering the E-modes first, one has to ensure that the E_r and E_Φ components vanish at $\theta = \theta_0$. Therefore it is required that

$$P_\nu^m(\cos\theta_0) = 0 \qquad r_1 < r < r_2,\ 0 \leqq \Phi < 2\pi. \tag{9}$$

At the topplate ($r = r_2$) and at the bottomplate ($r = r_1$) the E_θ and E_Φ components are tangential and must vanish, which leads to a system of two equations:

$$\frac{d}{dr} \left(\sqrt{\frac{\pi kr}{2}}\, (J_{\nu+1/2}(kr) + aN_{\nu+1/2}(kr)) \right)_{\substack{r=r_1 \\ r=r_2}} = 0 \tag{10}$$

or

$$\begin{pmatrix} B_\nu(k, r_1) & C_\nu(k, r_1) \\ B_\nu(k, r_2) & C_\nu(k, r_2) \end{pmatrix} \begin{pmatrix} 1 \\ a \end{pmatrix} = \begin{pmatrix} 0 \\ 0 \end{pmatrix} \tag{11}$$

where the abbreviations

$$B_\nu(k, r) = \sqrt{\frac{2\pi k}{r}}\, J_{\nu+1/2}(kr) + \sqrt{\frac{\pi kr}{2}}\, k \cdot J'_{\nu+1/2}(kr)$$

and

$$C_\nu(k, r) = \sqrt{\frac{2\pi k}{r}}\, N_{\nu+1/2}(kr) + \sqrt{\frac{\pi kr}{2}}\, k \cdot N'_{\nu+1/2}(kr)$$

have been introduced.

Equation (9) determines a set of possible values for the parameter ν for each m, which are marked with index numbers i, i.e. ν_{mi}, starting with the first ν that doesn't satisfy (9) identically. The determinant of the system (11) is set to zero in order to satisfy the equations simultaneously

$$B_\nu(k, r_1) C_\nu(k, r_2) - B_\nu(k, r_2) C_\nu(k, r_1) = 0. \tag{12}$$

This is the characteristic equation for the eigenvalues k to each index combination of m and i. The nth root of (12) is therefore marked with three indices $k_{m,i,n}$.

Considering the components for the H-modes leads to the condition:

$$\frac{d}{d\theta} [P_\nu^m(\cos\theta)]_{\theta=\theta_0} = 0 \tag{13}$$

for the ν-parameters to each m-value and to the characteristic equation

$$J_{\nu+1/2}(kr_1)N_{\nu+1/2}(kr_2) - J_{\nu+1/2}(kr_2)N_{\nu+1/2}(kr_1) = 0 \tag{14}$$

which defines the eigenvalues $k_{m,i,n}$.

The most often used modes are H-modes with the first index set to zero. Setting $m = 0$ reduces (5) to

$$E_r \equiv 0 \quad H_r = \frac{1}{j\omega\mu_0}\left(\frac{\partial^2 \Psi^H}{\partial r^2} + k^2 \Psi^H\right)$$

$$E_\theta = \frac{-1}{r \sin\theta}\frac{\partial \Psi^H}{\partial \Phi} \equiv 0 \quad H_\theta = \frac{1}{j\omega\mu_0 r}\frac{\partial^2 \Psi^H}{\partial r\, \partial\theta}$$

$$E_\Phi = \frac{1}{r}\frac{\partial \Psi^H}{\partial \theta} \quad H_\Phi = \frac{1}{j\omega\mu_0 r \sin\theta}\frac{\partial^2 \Psi^H}{\partial r\, \partial\Phi} \equiv 0. \tag{15}$$

More explicitly this can be written as

$$E_r \equiv 0$$

$$E_\theta \equiv 0$$

$$E_\Phi = \frac{E_0}{r}\sqrt{\frac{\pi kr}{2}}\left(J_{\nu+1/2}(kr) + bN_{\nu+1/2}(kr)\right)\frac{d}{d\theta}P_\nu(\cos\theta)$$

$$H_r = \frac{E_0}{j\omega\mu_0}\left\{\frac{d}{dr^2}\left[\sqrt{\frac{\pi kr}{2}}J_{\nu+1/2}(kr) + b\sqrt{\frac{\pi kr}{2}}N_{\nu+1/2}(kr)\right] + k^2\left[\sqrt{\frac{\pi kr}{2}}J_{\nu+1/2}(kr) + b\sqrt{\frac{\pi kr}{2}}N_{\nu+1/2}(kr)\right]\right\}P_\nu(\cos\theta)$$

$$H_\theta = \frac{E_0}{j\omega\mu_0 r}\left\{\frac{d}{dr}\left[\sqrt{\frac{\pi kr}{2}}J_{\nu+1/2}(kr) + b\sqrt{\frac{\pi kr}{2}}N_{\nu+1/2}(kr)\right]\right\}\cdot\frac{d}{d\theta}P_\nu(\cos\theta)$$

$$H_\Phi \equiv 0; \qquad b = -\frac{J_{\nu+1/2}(kr_1)}{N_{\nu+1/2}(kr_1)} = -\frac{J_{\nu+1/2}(kr_2)}{N_{\nu+1/2}(kr_2)}. \tag{16}$$

For computational purposes it is advantageous to avoid the resulting derivatives in (16) by using the relations

$$\frac{d}{dx}J_\alpha(x) = J_{\alpha-1}(x) - \frac{\alpha}{x}J_\alpha(x)$$

$$\frac{d}{dx}N_\alpha(x) = N_{\alpha-1}(x) - \frac{\alpha}{x}N_\alpha(x)$$

$$\frac{d}{dx}P_\alpha(x) = (1-x^2)^{-1}\alpha(P_{\alpha-1}(x) - xP_\alpha(x)). \tag{17}$$

Then it is only necessary to have appropriate subroutines for the special functions itself, which are available commercially. Equation (16) shows clearly one advantage of the H_{0in}-modes, namely the purely circumferential surface currents due to the fact that the H_Φ component is identical zero.

III. Numerical Results

Figs. 2 to 4 show useful mode charts for the design of truncated conical cavities with the angle θ_0 as parameter and the ratio $(D/L)^2$ as independent variable. Figs. 5 and 6 show mode charts with the ratio $(D/L)^2$ as parameter and the angle θ_0 as independent variable.

The scales in Figs. 2–4 are chosen exactly as in the usual mode charts for cylindrical cavities [7], i.e., the x-axis is scaled by $(D/L)^2$ and the y-axis is scaled by $(f_0 \cdot D)^2$, where f_0 is the resonance frequency. The charts start with full cones at a value $(D/L)^2 = \tan^2\theta_0$ and approach more and more the circular cylinder chart with increasing $(D/L)^2$. The mode charts depicted in Figs. 5 and 6 start with cylinders at $\theta_0 = 0$ and end with cones at $\theta_0 = \arctan(D/L)$. In Figs. 7 and 8, the dependence of the important H_{011} mode on the parameter $(D/L)^2$ and θ_0 is clearly apparent.

A figure of merit for cavities is the unloaded quality factor Q_0 defined by

$$Q_0 = \frac{2\pi f_0(\text{energy stored in circuit})}{\text{average power loss}} = \frac{2\pi f_0 \epsilon_0 \iiint |E|^2\, dv}{\iint R_s |H|^2\, da} \tag{18}$$

were f_0 is the resonance frequency and R_s the surface resistance of the cavity. The Q_0-value for the H_{011} mode was calculated and normalized results are given in Fig. 9 with the angle θ_0 as parameter and the ratio (D/L) as independent variable.

IV. Principle of Measurement

For the application of the cavity to measure surface resistance, it is necessary to determine the unloaded quality factor Q_0 very precisely. Simple computer simulations show that transmitted signals are much less sensitive to nonideal feeding lines than reflected signals. Therefore a transmission type cavity is the better choice, although two feeding lines are necessary. Fig. 10 shows a schematic block diagram, where a_1 and a_2 denote the attenuations of the feeding lines.

The Q_0 value is extracted from the formula

$$Q_0 = 2 \cdot \frac{1 - r_0}{1 - r_0^2 - t_0^2} Q_L \tag{19}$$

where r_0 is the magnitude of the reflection coefficient at the first feeding line and t_0 is the magnitude of the transmission coefficient, both determined at the resonance frequency f_0. Q_L is the loaded quality factor and is related to

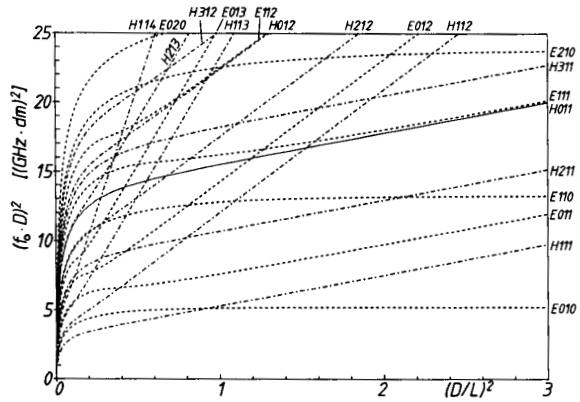

Fig. 2. Mode chart. $\theta_0 = 5°$.

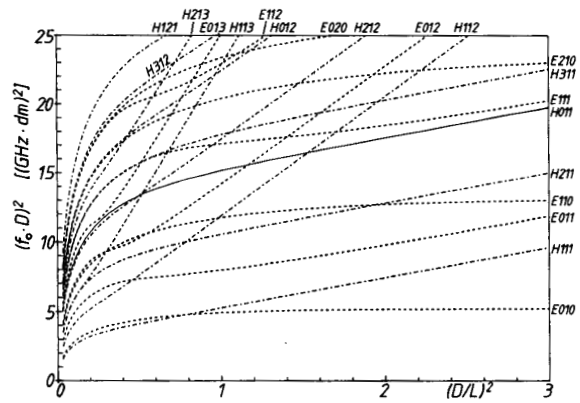

Fig. 3. Mode chart. $\theta_0 = 10°$.

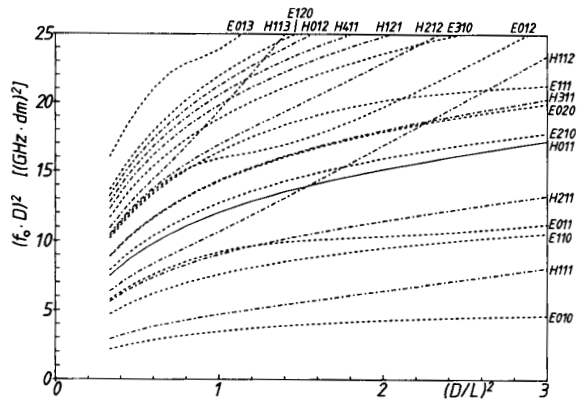

Fig. 4. Mode chart. $\theta_0 = 30°$.

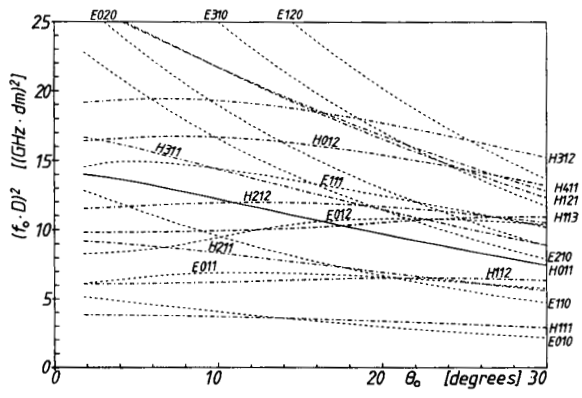

Fig. 5. Mode chart. $(D/L)^2 = 1/3$.

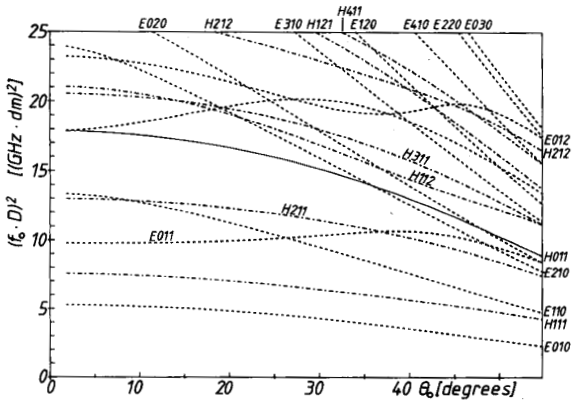

Fig. 6. Mode chart. $(D/L)^2 = 2$.

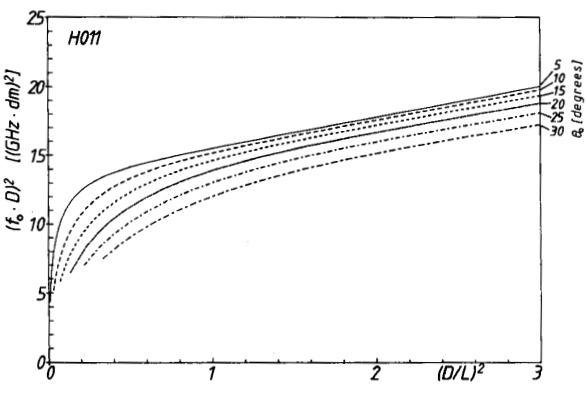

Fig. 7. H_{011}-mode in detail.

the transmitted signal by

$$\frac{|S_{21}(f)|^2}{|S_{21}(f_0)|^2} = \frac{1}{1 + Q_L^2 \left(\frac{f}{f_0} - \frac{f_0}{f}\right)^2} \tag{20}$$

In case of lossy but otherwise ideal feeding lines, r_0 and t_0 are related to the measured data by r_0[dB] = $|S_{11}|$ [dB] $- 2 \cdot a_1$[dB] and t_0[dB] = $|S_{21}|$ [dB] $- a_1$[dB] $- a_2$[dB]. A very precise way to determine the loaded quality factor Q_L is to fit the measured trace $|S_{21}(f)|$ to the theoretical shape over a significant bandwidth, for instance by applying the method of least squares.

However, in practice, the situation is more complicated. The cavity has to be evacuated and vacuumtight connectors have to be used. The feeding lines suffer from

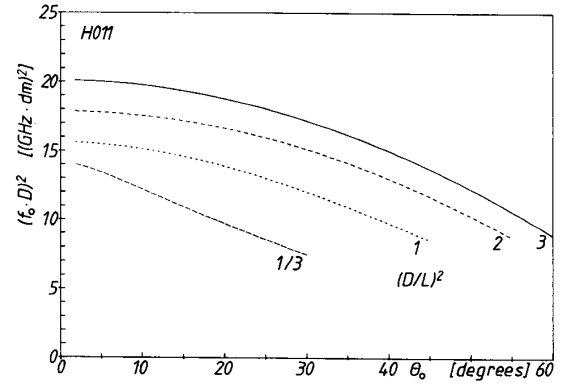

Fig. 8. H_{011}-mode in detail.

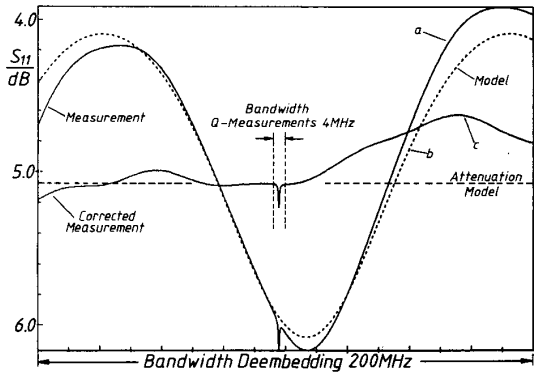

Fig. 11. Amplitude of $S11$. Resonance frequency f_0 = 18 GHz. Measured data, model data and deembedded data.

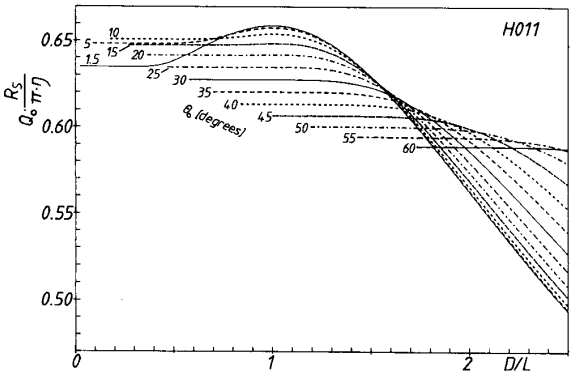

Fig. 9. Normalized Q_0-values for the H_{011} resonance. η: free space characteristic impedance. R_s: surface resistance.

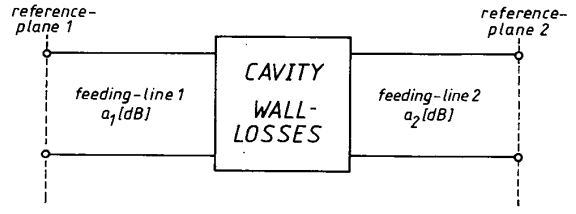

Fig. 10. Transmission type cavity.

multiple reflections between the nonideal connectors and the cavity, which leads to a systematic error. To minimize phase variations, stainless steel coaxial airlines are used. The inner conductor is coated with copper to minimize losses and is held by compensated PTFE holders one each per 16 cm line length. The discontinuities caused by the PTFE holders are negligibly small, but the transition between the airlines and the connectors could be compensated only partly by a short line length with a thinner inner conductor. A small fringing capacitance of about 30 fF remains. This small reactance causes a ripple of about ± 1 dB in the magnitude of S11, as can be seen from curve (*a*) of Fig. 11. It is difficult to determine the reflection coefficient r_0 of the cavity from such data because of the inclined curve in the vicinity of the resonance, and moreover to determine the correct attenuations of the feeding lines. To minimize this error, a deembedding technique was developed which is described below.

V. Deembedding Procedure

The model used for the connector and the feeding lines is sketched in Fig. 12. Parameters are physical air line length l, attenuation a, phase velocity inside connector v_{ph}, velocity of light c, length of connector l_c, and fringing capacitance of connector C. The coupling structure together with the cavity far outside resonance is modeled by a load inductance L. Whereas the length l is known, the parameter l_c, C, a and L have to be determined empirically.

Initial values for theses unknowns are easily derived by comparing the measurements with a computer simulation. Best values are derived by fitting the model traces onto the measured traces which is done in two steps. In a first step, the amplitude measurement of S_{11} is used and the model parameters except the connector length are adjusted so that measured and simulated data coincide as close as possible far outside resonance over a large bandwidth of about 200 MHz (Fig. 11(b)). In a second step, the connector length is determined by matching the phases obtained from the measurement and the model also far outside resonance. Since now all model parameters are known, one can deembed the measurements.

The deembedding process is carried out in various steps, as is visualized in Fig. 13. Starting from the reference planes of the measurements (RPM), the reference planes are shifted to the location of the connector capacitances C_1 and C_2. Then reactances are connected in parallel for compensation and ultimately the reference planes are shifted back to the original place. The last step is not necessary for the evaluation but is convenient in order to verify that the deembedding is done properly. The corrected measurements are shown in Fig. 11(c). Fig. 14 shows the effect of deembedding for the corresponding transmitted signal over a small bandwidth of 4 MHz.

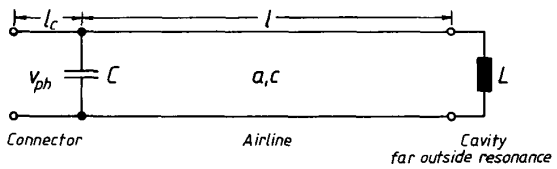

Fig. 12. Model of feeding line far outside resonance.

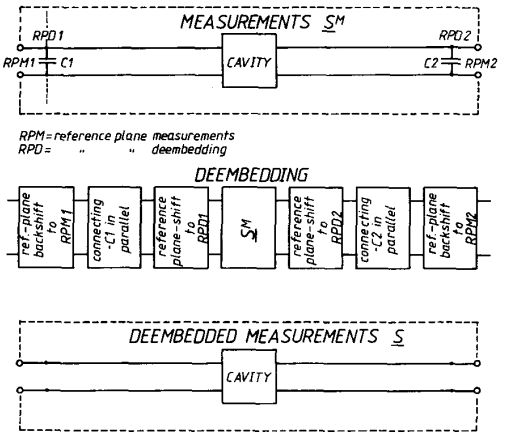

Fig. 13. Deembedding process.

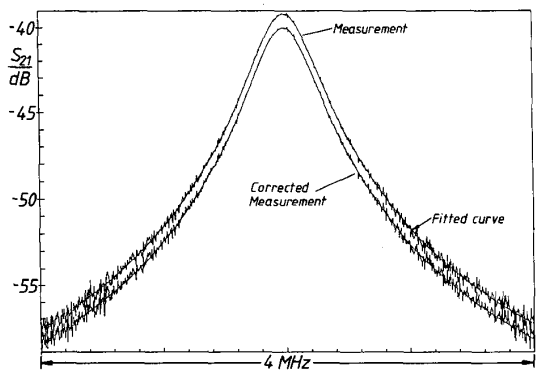

Fig. 14. Amplitude of $S21$. Resonance frequency f_0 = 18 GHz. Measured data and deembedded data.

VI. Surface Resistance Measurements

A block diagram of the experimental setup and a cross-section of the cavity for surface resistance measurements of high temperature superconductors (HTSC) is shown in Fig. 15. Best suited as working modes are the H_{0in} modes because they have only circumferential surface currents as mentioned before. In the present case the H_{011} mode is used. The cavity has been manufactured from copper and consists of three parts, the topplate, the jacket and the sample holder. The cover of the sample holder acts as the bottom plate and the sample is pressed against a concentric circular aperture of 9 mm diameter. This ensures that no currents flow across the sample boundary. The bottom- and topplate do not need to be in direct contact with the

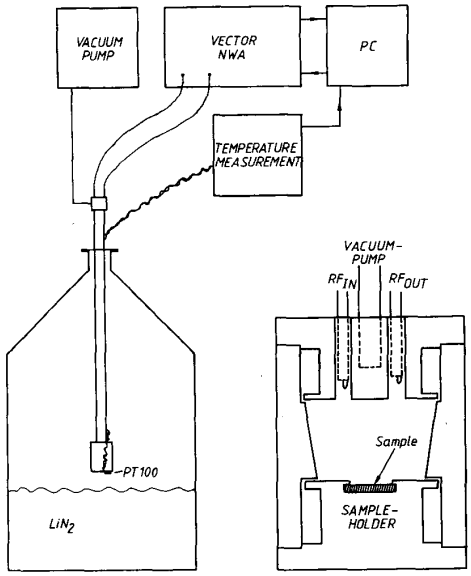

Fig. 15. Block diagram of experimental apparatus and cross-section of cavity.

jacket and therefore small gaps can be tolerated. For ease of fabrication the top plate and the coverplate of the sample holder were made of planar instead of spherical shape. The influence of this simplification on Q_0 and f_0 is negligible for practical cavities because small angles θ_0 and proper (D/L)-ratios are used.

The design depends on the sample size, expected Q values, resonance frequency and other requirements due to the cooling apparatus. Because the cavity is manufactured for the working mode H_{011}, the minimum frequency difference between the H_{011} and the E_{111} mode depends mainly on the low Q or large bandwidth of the latter. A set of possible combinations of the angle θ_0 and the (D/L) ratio for a given frequency difference can be taken from Fig. 16. In most practical cases, a small angle will be sufficient because of high Q-values.

The degree of the E_{111}-mode-detuning is not the only requirement to be put on the cavity. Another important item for surface resistance measurements is related to the relative portion of losses caused by the sample as given below.

The surface resistance is extracted from the unloaded quality factor Q_0 according to the formula

$$Q_0 = \frac{C}{R_{su} \cdot A + R_{sa} \cdot B} \tag{21}$$

where

$$C = 2\pi f_0 \epsilon_0 \int_V |E|^2 \, dv, \quad V = \text{volume of cavity}$$

$$B = \int_{Sa} |H_t|^2 \, da, \quad Sa = \text{surface of sample}$$

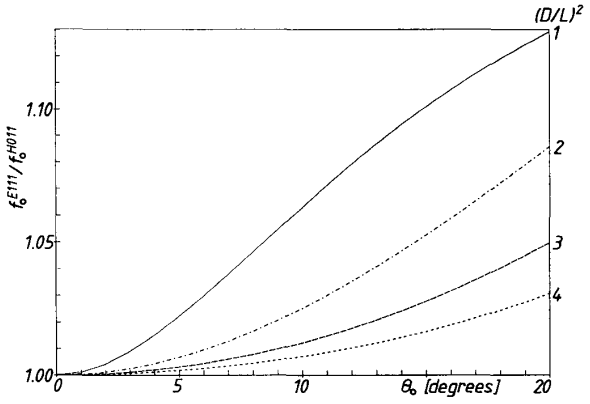

Fig. 16. Ratio of resonance frequencies E_{111}/H_{011}.

TABLE I
ANALYSIS OF SENSITIVITY: $\theta_0 = 9°$, $D = 23.34$ mm, $(D/L)^2 = 2$, $|dQ_0/Q_0| = 3 \cdot 10^{-3}$, $f_0 = 18$ GHz

No.	Cavity Material	Effective Sample ϕ	A/B	Order of Mag. R_{Sa}	Sensitivity	Comment
1	Copper, 77 K R_{Su} = 20 mΩ	9 mm	35.7	4 mΩ	4 mΩ ± 2.1 mΩ	10 mm · 10 mm quadratic sample
2	Copper, 77 K R_{Su} = 20 mΩ	20.7 mm	8.1	1 mΩ	1 mΩ ± 0.5 mΩ	sample = bottomplate
3	Copper, 77 K R_{Su} = 20 mΩ	25.9 mm	3.6	0.4 mΩ	0.4 mΩ ± 0.2 mΩ	sample = topplate
4	Niobium, 4.2 K R_{Su} = 0.05 mΩ	9 mm	35.7	0.1 mΩ	0.1 mΩ ± 0.005 mΩ	superconducting cavity

$$A = \int_{Su} |H_t|^2 \, da, \qquad \begin{aligned} Su &= \text{surface of cavity except sample surface} \\ H_t &= \text{tangential } H\text{-fields.} \end{aligned} \tag{22}$$

A, B, and C can be calculated from the theoretical expressions given in Section II. R_{Su} is the surface resistance of the cavity material and is determined by replacing the sample by a copper reference, i.e., the cavity has a homogeneous surface. A useful formula for the measurement sensitivity is derived from (21) by carrying out the total derivative.

This leads to

$$\left|\frac{dR_{Sa}}{R_{Sa}}\right| = \left(1 + \frac{AR_{Su}}{BR_{Sa}}\right)\left|\frac{dQ_0}{Q_0}\right| \tag{23}$$

As can be seen, a geometry dependent ratio A/B occurs in the calculation of the relative error in surface resistance. To minimize the error by choice of the geometry, this ratio must be as small as possible.

Ultimately a copper cavity was used with $\theta_0 = 9°$, $D = 23.34$ mm and $(D/L)^2 = 2$. The theoretical resonance frequencies are 17.986 GHz for the H_{011}-mode and 18.359 GHz for the E_{111}-mode. The frequency difference between the two modes of 373 MHz is not required to be so large, but the geometry is advantageous for the other requirements. Measurements yield a resonance frequency of 18.078 GHz and a copper surface resistance of 19.39 mΩ at 77.27 K.

Using (23) one can estimate the sensitivity of the cavity and assess the measurement accuracy. Table I shows calculated results for some interesting configurations based on an achieved relative accuracy of the Q_0 measurement of $3 \cdot 10^{-3}$. This value depends on the stability of the cavity construction, the cooling equipment employed and on the microwave S-parameter measurement set-up used.

The table shows that the measurement accuracy is about ±2.1 mΩ for small 10 mm × 10 mm samples with a surface resistance in the order of 4 mΩ, i.e., one fifth of the cavity material copper. When the surface resistance is smaller a larger sample area is necessary or ultimately a superconducting cavity must be used. Another possibility is to characterize the films at higher frequencies because of the anticipated degradation of HTSC-surface conductivity governed by an f^2-law [8] in comparison with the $f^{1/2}$-law for copper in the normal skin effect regime, or the $f^{2/3}$-law for copper in the anomal skin effect regime. Example: if only 10 mm × 10 mm samples are available, one can replace both bottom- and topplate in a cavity with $\theta_0 = 7.5°$, $(D/L)^2 = 1.8$ and $D = 7.98$ mm. The resonance frequency is then 52 GHz and the factor A/B is 2.4. Assuming a copper surface resistance of 40 mΩ, a sample surface resistance in the range of 10 mΩ and an

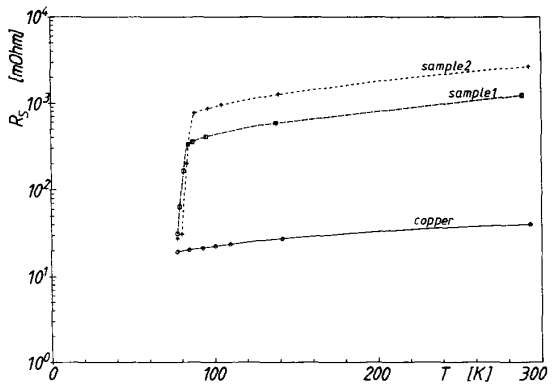

Fig. 17. Measured temperature dependence of $YBa_2Cu_3O_x$ on MgO manufactured by means of magnetron sputtering. Film thicknesses unknown.

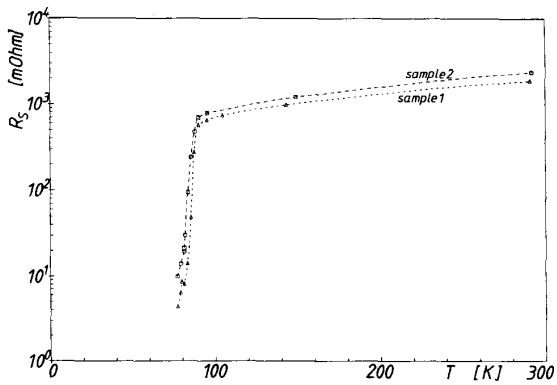

Fig. 18. Measured temperature dependance of $YBa_2Cu_3O_x$ on MgO manufactured by means of laser ablation. Film thicknesses approximately 300 nm.

accuracy of the Q_0 measurement of $20 \cdot 10^{-3}$ leads to a sensitivity of 10 mΩ ± 2.1 mΩ. The degraded accuracy of the Q_0-measurement is assumed, because often scalar measurement techniques are used at 52 GHz.

Various YBaCuO-films on 10 mm × 10 mm MgO substrates were measured at 18 GHz using a HP 8510A networkanalyzer and cooling in LN_2 down to a lowest temperature of 77 K. Fig. 17 shows measurements of the surface resistance versus temperature for two samples manufactured by means of magnetron sputtering [9]. It is assumed that the higher R_S values for sample 2 are due to a thinner film. Fig. 18 shows measurements of two films manufactured by means of laser ablation [10]. The film thicknesses are approximately 300 nm. The lowest measured value was 4.5 mΩ at 77 K, which is roughly one fifth of the copper reference value of 19.39 mΩ.

VII. Conclusion

A conical cavity is described. The new cavity is superior to the often used cylindrical cavity, because it intrinsically does not suffer from mode degeneration. This is especially advantageous for material measurements where the change in quality factor due to a sample is evaluated. A measurement setup to determine the surface resistance of high temperature superconductors is described. Results are given for various samples at 18 GHz. The lowest value obtained was 4.5 mΩ ± 2.1 mΩ.

Acknowledgment

We would like to thank Prof. U. Merkt and his group from the University of Hamburg for providing the samples manufactured by laser ablation and Dr. Dössel and his group from the Philips research laboratories Hamburg for providing the samples manufactured by magnetron sputtering.

References

[1] S. Sridhar, "Microwave response of thin-film superconductors," *J. Appl. Phys.*, vol. 63, no. 1, pp. 159–166, Jan. 1, 1988.
[2] J. S. Martens *et al.*, "Microwave surface resistance of $YBa_2Cu_3O_{6.9}$ superconducting films," *Appl. Phys. Lett.*, vol. 52, no. 21, pp. 1822–1824, May 23, 1988.
[3] N. Klein *et al.*, "Millimeter wave surface resistance of epitaxially grown $YBa_2Cu_3O_{7-x}$ thin films," *Appl. Phys. Lett.*, vol. 54, no. 8, pp. 757–759, Feb. 20, 1989.
[4] T. Konaka *et al.*, "Millimeter-Wave Surface Resistance of $EuBa_2Cu_3O_{7-y}$ Film on MgO Substrates," *Japan. J. Appl. Phys.*, vol. 29, no. 4, pp. L569–L571, Apr. 1990.
[5] R. F. Harrington, *Time-Harmonic Electromagnetic Fields*. New York: McGraw-Hill, 1961.
[6] I. S. Gradshteyn and I. M. Ryzhik, *Table of Integrals, Series and Products*. New York: Academic, 1980.
[7] W. Otto, "Berechnung von Hohlraumresonatoren höchster Kreisgüte," *Nachrichtentechnik*, vol. 10, 1960, H. 5, S. 205 (pt. I). *Nachrichtentechnik*, vol. 10, 1960, H. 6, S. 266 (pt. II). *Nachrichtentechnik*, vol. 10, 1960, H. 8, S. 365 (pt. III).
[8] H. Piel and G. Müller, "The microwave surface impedance of high-T_c superconductors," *IEEE Trans. Magn.*, vol. 27, no. 2, pp. 854–862, Mar. 1991.
[9] O. Dössel, private communication.
[10] U. Merkt, private communication.
[11] B. Mayer, R. Knöchel, and A. Reccius, "Novel Truncated Cone Cavity for Surface Resistance Measurements of High T_c Superconducting Thin Films," in *1991 IEEE MTT-S Int. Microwave Symp. Dig.* Boston, MA, pp. 1019–1022.

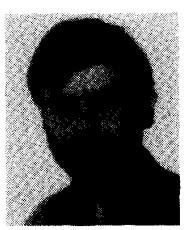

Bernd Mayer was born in Metzingen, near Stuttgart, Germany. He received the Dipl.-Ing. (FH) degree in telecommunications from the Fachhochschule für Technik Esslingen in 1984 and the Dipl.-Ing. degree in electrical engineering from the Universität Bochum in 1987.

From 1987 to 1988, he was a Research Assistant at the Universität Paderborn. Since 1989, he has been a Research Assistant at the Technische Universität Hamburg-Harburg, Arbeitsbereich Hochfrequenztechnik.

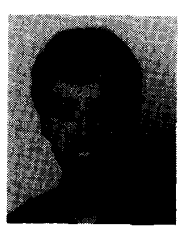

Andreas Reccius was born in Glückstadt, West Germany, on September 3, 1964. Since 1985 he has been studying physics at the University of Hamburg.

Currently he works at the Technical University of Hamburg-Harburg on microwave surface resistance of high temperature superconductors.

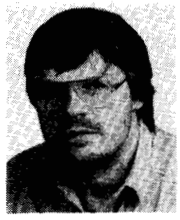

Reinhard Knöchel (SM'90) was born in Trittau, near Hamburg, Germany. He received the Dipl.-Ing. degree in 1975 and the Dr.-Ing. degree in 1980 in electrical engineering both from technical University of Braunschweig, Germany.

From 1975 to 1980 he was a Research Assistant at the Institut für Hochfrequenztechnik, Braunschweig, where he worked on microwave oscillators, oscillator noise theory, finline-components and evanescent-mode waveguide techniques. From 1980 to 1986 he was with Philips Research Laboratories, Hamburg, where his activities included again work on various microwave components, microwave hyperthermia, microwave system applications and heterodyne optical time domain reflectometry. In 1986 he joined the Technical University of Hamburg-Harburg, where he is currently a Professor. His research interests are in the design and fabrication of microwave components, microwave measurement systems and high temperature superconductivity.

Dr. Knöchel is a member of VDE/ITG. In 1978, he was corecipient of the NTG-prize, and in 1980 he received the Microwave Prize at the 10th European Microwave Conference.